Recent Progress in Application of Internal Oxidation Technique in Nb_3Sn Strands

Xingchen Xu, Xuan Peng, Michael Sumption and E. W. Collings

***Abstract*— The internal oxidation technique can generate ZrO_2 nano particles in Nb_3Sn strands, which markedly refine the Nb_3Sn grain size and boost the high-field critical current density (J_c). This article summarizes recent efforts on implementing this technique in practical Nb_3Sn wires and adding Ti as a dopant. It is demonstrated that this technique can be readily incorporated into the present Nb_3Sn conductor manufacturing technology. Powder-in-tube (PIT) strands with fine subelements (~25 μm) based on this technique were successfully fabricated, and proper heat treatments for oxygen transfer were explored. Future work for producing strands ready for applications is proposed.**

***Index Terms*— Nb_3Sn strands; internal oxidation; subelement design; heat treatment; oxygen transfer.**

I. Introduction

FOR areas or projects that require high-field magnets wound from Nb_3Sn strands, such as nuclear magnetic resonance (NMR) [1], proposed high-energy Large Hadron Collider (HE-LHC) [2] or Future Circular Collider (FCC) [3], improvement of high-field J_c of Nb_3Sn is still worth significant efforts as it dramatically influences the magnet design (e.g., coil width) and cost [4]. Taking the FCC project as an example, it requires an improvement of 16 T J_c by at least 50% relative to present Nb_3Sn strands [5]. The record J_cs of Nb_3Sn strands have plateaued since the early 2000s [6-7]. However, recently it was demonstrated [8-9] that an internal oxidation technique could be applied in Nb_3Sn strands to remarkably improve their performance. In this technique, the commonly-used pure Nb or Nb-7.5wt.%Ta alloy is replaced by Nb-Zr (or another Nb alloy with the solute having much stronger affinity to oxygen than Nb does), and oxide powder (e.g., CuO, SnO_2, or Nb_2O_5, etc.) is introduced in proper structures for supplying sufficient oxygen to the Nb-Zr alloy during heat treatment but prior to the reaction between Nb with Sn. The Zr atoms are selectively oxidized to form ZrO_2 nano particles in the Nb (or Nb_3Sn) matrix during heat treatment. These ZrO_2 particles significantly refine Nb_3Sn grain size: it was shown that such samples reacted at 625-650 °C have grain size of ~40 nm, one third of present-day Nb_3Sn strands (without grain refiners) after the same heat treatments. This leads to a huge gain in high-field J_c [9] because: 1) reduction in Nb_3Sn grain size boosts the flux pinning capacity by creating a higher density of grain boundaries as flux line pinning centers, and 2) the peak of pinning force F_p-B curve shifts from $0.2B_{c2}$ (where B_{c2} is the upper critical field at which J_c vanishes) to higher field (e.g., $0.34B_{c2}$ for a grain size of 35 nm [9]) as the Nb_3Sn grain size is refined to a certain level (presumably below ~50 nm [9,10]). Moreover, intra-granular ZrO_2 particles may also serve as point pinners.

The above results of refined grain size and boosted J_c were achieved in a "modified tube type" mono-filament in which SnO_2 powder is positioned between the Cu/Sn core and the Nb-1%Zr tube wall [8,9], so that Nb can reduce SnO_2 and take up its oxygen during heat treatment. The mono-filament was drawn down to ~200 μm filament size without breakage; however, further reduction led to filament distortion and breakage. Thus, it has been decided to pursue alternative subelement structures for implementing this internal oxidation technique. The feasibility of applying this technique in PIT strands was explored. Encouraging results were obtained: such strands could be drawn well to get very fine subelement size (25 μm), and only a small amount of oxide was required to fully oxidize the Nb-1%Zr alloy and markedly refine grain size. It was also found that the heat treatment schedule is critical for oxygen transfer. We also attempted to introduce Ti as a dopant for B_{c2} improvement.

II. An Experiment to Add Titanium

Although a doubling of 12 T Nb_3Sn layer J_c was achieved in [9], the performance can be further improved, considering that the B_{c2} of the sample with doubled J_c was not yet optimized (~20 T at 4.2 K), primarily due to two reasons: under-reaction in the large subelement and lack of Ta or Ti dopants [9]. Thus, experiments of adding Ti dopant to that strand were conducted. Based on the success of using Sn-Ti alloy in conventional tube type [11] and rod-in-tube [12] strands, we continued using Sn-Ti alloy as Sn core and increased the Ti content to 6 at.% (intending to introduce 1.5 at.% Ti into the Nb_3Sn). Back-scatter electron (BSE)/scanning electron microscopy (SEM) image of such a strand is shown in Fig. 1 (a). Some fine Ti_6Sn_5 precipitates can be seen due to the supersaturation of Ti in Sn-Ti alloy.

The strand was heat treated at 650 °C for 150 hours (the temperature was increased from room temperature at a rate of

Manuscript received Sept. 5th, 2016. This work was supported in part by the U.S. Dept. of Energy, Office of High Energy Physics, SBIR phase I grant DE-SC0013849.

X. Xu is with the Fermi National Accelerator Laboratory, PO Box 500, MS 315, Batavia, IL 60510 USA (phone: 630-840-8388; e-mail: xxu@fnal.gov)

X. Peng is with Hyper Tech Research Inc., Columbus, Ohio, USA.

M. Sumption and E. Collings are with the Ohio State University, Columbus, Ohio USA.

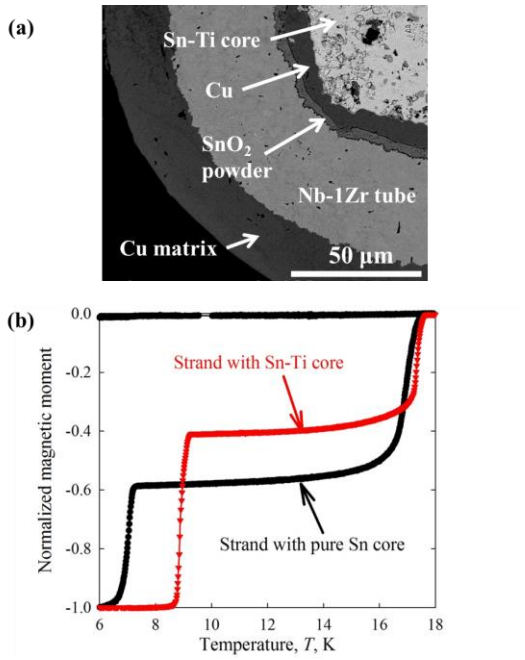

Fig. 1. (a) SEM image of the strand for Ti doping, and (b) *M-T* curves for the strands with and without Ti, both reacted at 650 °C for 150 hours.

50 °C/h without intermediate stages). It turned out, however, the grain size of this sample was nearly 100 nm, indicating that internal oxidation had not succeeded. To determine the content of oxygen absorbed by the Nb-1%Zr, magnetization vs temperature (*M-T*) curve at 5 mT of this reacted sample was measured using a vibrating sample magnetometer (VSM), recognizing that the critical temperature T_c of Nb alloy drops by 0.93 K for each at.% oxygen dissolved [13]. The normalized *M-T* curve of this reacted sample is shown in Fig. 1 (b), along with that of a control strand with the same structure but no Ti in the Sn core. The results indicated that less than 0.5 at.% oxygen was absorbed by Nb-1%Zr in the strand with Sn-Ti core, while over 2 at.% oxygen was absorbed in the control sample with pure Sn core, as calculated from the *M-T* curves of the residual Nb-1%Zr in Fig. 1 (b). This indicates that the addition of Ti in the Sn core prevented oxygen transfer from SnO_2 to Nb-1%Zr.

A possible reason is that during heat treatment after liquid Sn-Ti and Cu mixed, Ti in the core was exposed to the SnO_2 powder, so oxygen and Ti reacted to form TiO_2. This reaction was faster than the diffusion of oxygen into the Nb-Zr alloy. Since TiO_2 cannot be reduced by Nb (Ti has stronger affinity to oxygen than Nb does), it cannot serve as Ti source or oxygen source.

This experiment indicates that in order to add Ti, either the oxygen source or the Ti source has to be moved away from the Sn core, so that oxygen dissolves in Nb-1%Zr alloy before it reacts with Ti. A promising scheme is to distribute Nb-47Ti rods in the Nb alloy tube, which has been demonstrated to be feasible in conventional tubular strands [14].

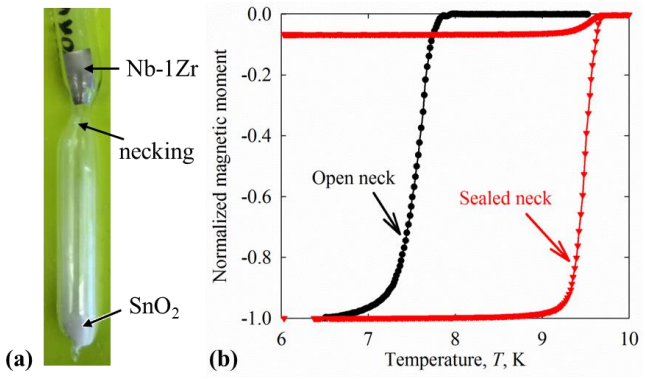

Fig. 2. (a) A photograph showing the quartz tube with open neck, and (b) *M-T* curves of the Nb-1%Zr pieces heat treated with open neck and sealed neck, respectively.

III. Oxygen Transfer in Strands

A. *Feasible Structures for Oxygen Transfer*

As mentioned earlier, the above "modified tube type" subelements are difficult to be drawn to small sizes (e.g., 50 μm). This is perhaps due to their five-layer structure, with a very thin layer of oxide powder in between (see Fig. 1 a). Therefore, in order to implement this internal oxidation technique in practical Nb_3Sn strands, we have to explore new subelement structures to enable the oxide powder to supply oxygen to Nb-Zr while retaining drawability. Meanwhile, it should be noted that oxygen transfer from oxide to Nb-Zr may be blocked if the subelement structure is not properly designed (e.g., [8]). The principle for oxygen transfer from oxide to Nb can be demonstrated by the following experiment.

As shown in Fig. 2 (a), SnO_2 powder was put at the bottom of a quartz tube, which was necked at a certain height above the powder so that: 1) a Nb-1%Zr piece can be constrained above the neck without contacting the oxide powder, and 2) the Nb-1%Zr and the SnO_2 powder share a common atmosphere through the neck. The quartz tube was pumped to high vacuum (~10^{-3} Pa) and then filled up with 200 torr of Ar and sealed. Then the tube was transferred to a furnace for heat treatment. It was found that oxygen could quickly transfer from the SnO_2 powder to the Nb-1%Zr strip, and with excess Nb-1%Zr, SnO_2 powder eventually lost all of its oxygen and transformed to Sn. *M-T* curve of the Nb-1%Zr piece after heat treatment shown in Fig. 2 (b) indicates that enough oxygen can be absorbed if the oxide powder is sufficient. On the other hand, in another tube with the neck sealed so that the atmosphere did not connect, the Nb-1%Zr failed to absorb any oxygen (Fig. 2 b). This experiment demonstrates that oxide powder and Nb-Zr do not need to be in contact for oxygen transfer to occur; as long as the atmosphere connects, oxide powder can supply oxygen to Nb alloy through atmosphere – most likely via equilibration of oxygen partial pressure in the space where atmosphere can reach.

TABLE I. MOLAR VOLUMES OF VARIOUS MATERIALS*

Material	Nb	Sn	$NbSn_2$	Nb_3Sn	SnO_2
Molar weight, g/mol	92.9	119	330	397	151
Mass density, g/cm^3	8.57 [15]	7.17 [15]	8.26 [16]	8.92	6.85 [17]
Volume per mol of molecure, cm^3/mol	10.8	16.6	40.0	44.6	21.8

*: The molar volume of pure, stoichiometric Nb_3Sn is calculated based on its A15 crystal structure with lattice constant of 0.529 nm [18]. The molar volumes of other materials are calculated by dividing their molar weights by their mass densities.

Following this principle, this internal oxidation technique can also be applied in rod-restack-process (RRP) (schemes described in [9]) and PIT strands, and in bronze-process or single-barrier internal-tin strands, in which each Nb filament is replaced by a Nb-1%Zr tube filled with oxide powder.

B. *Amount of Oxide Needed for Full Oxidation of Nb-1%Zr*

An important question is: does the addition of sufficient SnO_2 powder to fully oxidize the Nb-1%Zr alloy take so much space of the subelement cross sectional area that the fraction of Nb_3Sn formed is severely reduced? A calculation is given below. To supply just the right amount of oxygen (i.e., the number of moles of oxygen atoms is twice of that of Zr atoms), the ratio of the area of SnO_2 powder to that of the Nb-1%Zr equals to 1% of the ratio of the molar volume of SnO_2 to that of Nb-1%Zr, because approximately 0.01 mole of SnO_2 is needed to fully oxidize 1 mole of Nb-1%Zr. With the molar volumes of SnO_2 and Nb-1%Zr (which approximately equals to that of pure Nb) shown in Table I, the ratio of the area of SnO_2 to that of the Nb-1%Zr is calculated to be 2%, meaning that only 2% of the Nb alloy area (which itself normally takes 50-70% of the whole subelement area [19]) needs to be sacrificed for addition of sufficient SnO_2. In reality the required SnO_2 area fraction may be higher than 2% depending on the SnO_2 powder packing density. To verify this theoretical calculation, a special wire was fabricated, in which ~4% of Nb-1%Zr area was filled with SnO_2 powder (assuming the powder packing density to be 50%) to see if this amount of SnO_2 can supply sufficient oxygen. *M-T* curve of this sample after heat treatment at 500 °C shows a T_c between 6.5-7.5 K for the residual Nb-1%Zr, indicating that over 2 at.% oxygen had been absorbed by Nb-1%Zr. It is also worth pointing out that the reduction product of SnO_2 powder – Sn – can also react with Nb to form Nb_3Sn.

IV. Application to PIT Strands

A. *Drawability of PIT Strands with This Technique*

Implement of this technique in PIT strands does not need modification of subelement structure: the oxide powder can be blended with Sn source powders in the core – such a three-layer structure is advantageous for wire drawing. Fig. 3 shows a 48/61-filament PIT strand along this line fabricated in Hyper Tech Research Inc. and was drawn down to 0.254 mm without breakage, which leads to a subelement diameter of 25 μm. PIT strands with 120 filaments were fabricated in SupraMagnetics Inc. and drawn to a size with subelement diameter of ~50 μm.

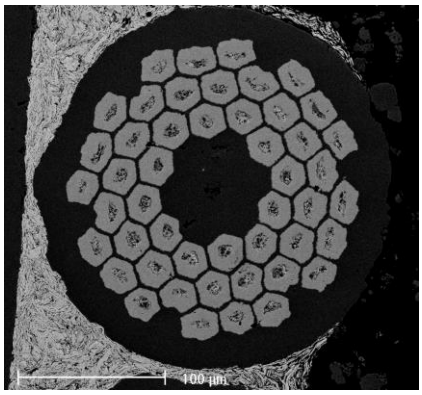

Fig. 3. SEM image of a unreacted 48/61-filament PIT strand fabricated with Sn source and oxide powders mixture in Nb-1%Zr tubes.

B. *Optimization of Heat Treatment for PIT Scheme*

For the PIT strands, it was found that oxygen transfer was sensitive to the heat treatment schedule. Fig. 4 (a) and (b) show secondary electron (SE)/SEM images of fractured surfaces of a PIT strand heat treated at 625 °C with ramp rates of 50 °C/h and 10 °C/h, respectively. The sample with the slow temperature ramp rate during heat treatment has grain size of <40 nm, while that of the sample with the fast ramp rate is 60-70 nm. *M-T* measurement (Fig. 4 c) shows that the Nb-1%Zr in the sample with the fast ramp rate failed to absorb sufficient oxygen. Since the amount of SnO_2 powder in this PIT strand contains sufficient oxygen to fully oxidize the Nb-1%Zr, why did temperature ramp rate influence the amount of oxygen taken by Nb-1%Zr? A possible explanation is that the formation of Nb-Sn intermetallic compounds (including $NbSn_2$, Nb_6Sn_5, and Nb_3Sn) in the inner side of the Nb-1%Zr tube may block the oxygen transfer. It is well known that oxygen atoms have a high diffusivity in metals because they can diffuse through interstitial voids. The atomic packing

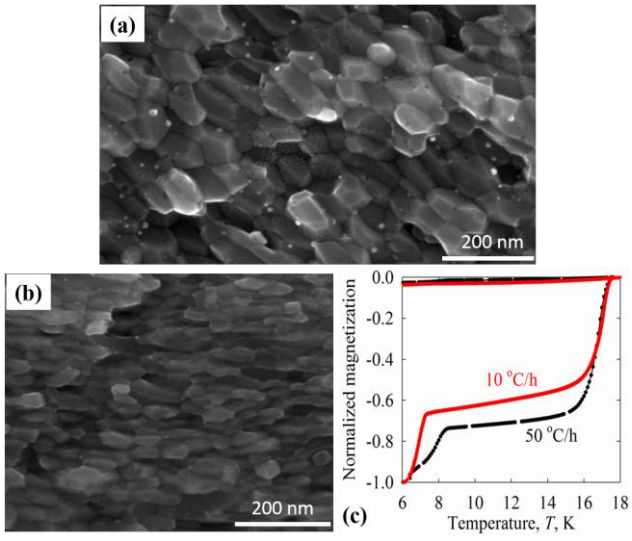

Fig. 4. SEM images of fractured surfaces of a PIT strand heat treated at 625 °C with ramp rates of (a) 50 °C/h and (b) 10 °C/h, respectively; (c) *M-T* curves of the strand heat treated with different temperature ramp rates.

factor of Nb, which has a body-centered cubic (bcc) crystal structure, is only 68%. On the other hand, crystal structures of intermetallic compounds are known to have much higher atomic packing factors. A simple calculation may help to clarify this. For instance, using the data in Table I, the total volume of 3 moles of Nb and 1 mole of Sn is 3×10.8+16.6 =49 cm^3, ~10% larger than the volume of 1 mole of Nb_3Sn (44.6 cm^3), meaning that the total volume shrinks as Nb and Sn transform to Nb_3Sn. The closer-packed structure means lower void fraction, which is disadvantageous for oxygen diffusion. This is also true for $NbSn_2$ and Nb_6Sn_5.

Thus, one possible problem with the PIT scheme (in which oxide powder is blended with Sn source powders in the core) is the competition between outward diffusion of Sn and outward diffusion of oxygen because Nb-Sn reaction already starts at low temperatures (below 400 °C [20]) where oxygen transfer rate is still low. Once an intact Nb-Sn intermetallic compound layer forms at the inner surface of the Nb alloy tube, it begins to block the atmosphere connection between the oxide powder and the unreacted Nb alloy, and thus terminate oxygen transfer. As revealed by the in-situ X-ray diffraction (XRD) measurements [21] and metallographic observations [22], as the high-Sn Cu-Sn (or other Sn sources with high activities of Sn) reacts with Nb, a Cu-Nb-Sn phase first forms below 400 °C [20,21], which begins to transform to $NbSn_2$ phase as the temperature reaches ~490 °C [21], which transforms to Nb_6Sn_5 and then Nb_3Sn phases sequentially at higher temperatures later. For now, it is not certain whether the Cu-Nb-Sn layer permits oxygen to diffuse through; however, it is unlikely that oxygen can diffuse across the $NbSn_2$ layer. Since high temperatures favor the formation of Nb-Sn intermediate layers, a slower ramp rate delays the formation of these compounds and thus provides more time for oxygen transfer before it is cut off.

A cure to this problem is to adjust the composition of powders in the core, e.g., by increasing the amount of oxide, so that the oxygen supply rate is higher and the formation rate of Nb-Sn intermediate phases is slower. Another possible solution is to add a pre-heat treatment stage at a temperature below the formation temperature of $NbSn_2$, provided that the Cu-Nb-Sn ternary phase allows for oxygen transfer. Experiments of 450 °C showed positive results with fully refined grain size.

C. Problems with Present PIT Strands and Future Work

Although significant progress has been made on implementing the internal oxidation technique on PIT strands, some practical problems have been identified for the PIT strands fabricated so far. Fig. 5 shows the *M-T* curve of the 48/61-subelement PIT strand shown in Fig. 3 after heat treatment at 450 °C for 50 hours and then at 660 °C for 120 hours, and SE images of fractured surfaces of its two subelements. Clearly a subelement has refined grain size of ~50 nm (Fig. 5 c), while that of another subelement is ~80 nm (Fig. 5 d). The *M-T* curve of this multi-filamentary PIT strand after reaction (Fig. 5 a) shows a very broad superconducting transition (6.5-8.5 K) associated with the residual Nb-1%Zr,

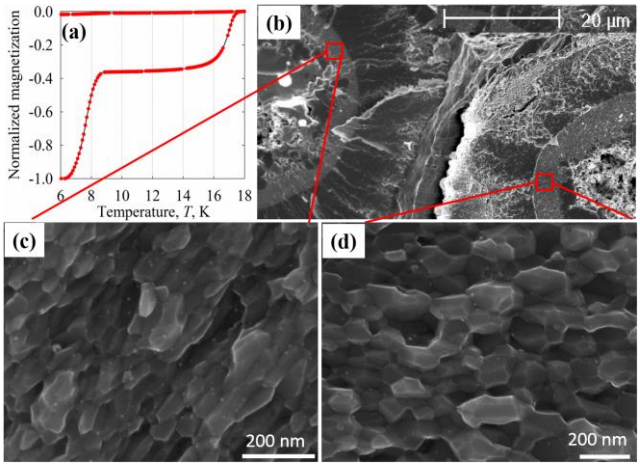

Fig. 5. (a) *M-T* curves of the 48/61-subelement PIT strand shown in Fig. 3 after heat treatment at 450 °C for 50 hours and then at 660 °C for 120 hours, and (b)-(d) SE images of fractured surfaces of this strand.

indicating that oxygen contents in Nb-1%Zr of different filaments vary significantly. Analysis of the BSE images of the unreacted strand indicates that this variation of oxygen contents may originate from filament-to-filament variation in SnO_2 amounts. As mentioned in section III, oxygen partial pressure can be equilibrated in a certain range, so it is most likely that macro-inhomogeneity of oxide distribution among the filaments caused this phenomenon. A possible cause is as follows. For the fabrication of the above strand, SnO_2 powder with particle sizes below 100 nm and Sn source powders with micron-size or 325-mesh particles were used. During the mixing of these powders, particles of different sizes tend to separate. Furthermore, after the powder mixture is poured into a Nb-1%Zr tube, small particles tend to sink during the vibration needed for compaction. This causes non-uniform distribution of oxide powder along the tube length, and after the tube is drawn to a small size and cut into 48 pieces for restacking, different filaments would have different oxide amounts. Apparently, to fabricate practical strands, this problem must be solved.

Another problem with the 48/61-filament strand shown in Fig. 3 is that the fractions of the precursors (Nb-1%Zr, oxide and Sn source powders) have not been optimized yet. Optimal ratios can certainly be calculated. However, some practical factors must be considered, such as reduction of inner diameter/outer diameter of the Nb-1%Zr tube during wire drawing, because the initial packing density of powders is low. More experiments are needed to solve this issue.

V. Summary

Experiments for adding Ti show that either oxygen or Ti source must be away from the Sn core to avoid formation of TiO_2. It is revealed that oxygen transfer can occur via atmosphere between oxide powder and Nb-1%Zr, while contact between them is not required. Fabrication of PIT strands with fine filaments was successful, and proper heat treatments were proposed for oxygen transfer. However, there

are still some problems to be solved in order for present PIT strands to be practically applicable.

REFERENCES

[1] T. Kiyoshi *et al.*, "Development and operation of superconducting NMR magnet beyond 900 MHz", *IEEE Trans. Appl. Supercond.*, vol. 11, Issue 1, Pages 2347-2350, May 2001.

[2] L. Rossi and E. Todesco, "Conceptual design of 20 T dipoles for high-energy LHC," arXiv:1108.1619, 2011.

[3] A. Ballarino and L. Bottura, "Targets for R&D on Nb_3Sn Conductor for High Energy Physics", *IEEE Trans. Appl. Supercond.*, vol. 25, Issue 3, 6000906, Jan. 2015.

[4] S. Caspi and P. Ferracin, "Limits of Nb_3Sn accelerator magnets", *Particle Accelerator Conference*, pp. 107-111, 2005.

[5] M. Benedikt, "FCC – High Energy Collider", Applied Superconductivity Conference 2016 Plenary presentation, Sept. 6th, 2016.

[6] J. A. Parrell, Y. Zhang, R. W. Hentges, M. B. Field, and S. Hong, "Nb_3Sn strand development at Oxford Superconducting Technology", *Adv. Cryo. Engr.*, vol. 48, pp. 968-977, 2002.

[7] M. B. Field, Y. Zhang, H. Miao, M. Gerace, and J. A. Parrell, "Optimizing Nb_3Sn Conductors for High Field Applications", *IEEE Trans. Appl. Supercond.*, vol. 24, Issue 3, 6001105, June 2014.

[8] X. Xu, M. D. Sumption, X. Peng, and E. W. Collings, "Refinement of Nb_3Sn grain size by the generation of ZrO_2 precipitates in Nb_3Sn wires", *Appl. Phys. Lett.*, Vol. 104, Issue 8, Pages 082602, Feb. 2014.

[9] X. Xu, M. D. Sumption, and X. Peng, "Internally Oxidized Nb_3Sn Strands with Fine Grain Size and High Critical Current Density", *Adv. Mater.*, Vol. 27, Issue 8, Pages 1346-1350, Feb. 2015.

[10] D. R. Dietderich and A. Godeke, "Nb_3Sn research and development in the USA - Wires and cables", Cryogenics, Vol. 48, Issue 7-8, Pages 331-340, Aug. 2008.

[11] X. Xu, E. W. Collings, M. D. Sumption, C. Kovacs, and X. Peng, "The Effects of Ti Addition and High Cu/Sn Ratio on Tube Type $(Nb,Ta)_3Sn$ Strands, and a New Type of Strand Designed to Reduce Unreacted Nb Ratio," *IEEE Trans. Appl. Supercond.*, vol. 24, Issue 3, 6000904, Jun. 2014.

[12] X. Xu, M. D. Sumption, and E. W. Collings, "Influence of Heat Treatment Temperature and Ti doping on Low Field Flux Jumping and Stability in $(Nb-Ta)_3Sn$ Strands," *Supercond. Sci. Technol.*, Vol. 26, Issue 7, 075015, July 2013.

[13] C. C. Koch, J. O. Scarbrough and D. M. Kroeger, "Effects of Interstitial Oxygen on Superconductivity of Niobium", *Phys. Rev. B*, Vol. 9, Issue 3, Pages 888-897, Feb.1974.

[14] C. V. Renaud, and T. Wong, "Titanium Doped Nb_3Sn Superconductor Fabricated by the Internal Tin Tube (ITT) Approach", *IEEE Trans. Appl. Supercond.*, Vol. 19, Issue 3, Pages 2548 – 2551, June 2009.

[15] ASM Handbook, "Properties and Selection: Nonferrous Alloys and Special-Purpose Materials", Vol. 02, ASM international, Pages 1099-1021, 1990.

[16] S. Naille et al., "Lithium insertion-deinsertion mechanism in $NbSn_2$ anode studied by ^{119}Sn Mossbauer spectroscopy", *Hyperfine Interact.*, Vol. 187, Pages 1105–1112, 2008.

[17] W. M. Haynes, "CRC handbook of chemistry and physics", CRC Press, Page 4-139, 2013.

[18] H. Devantay, J. L. Jorda, M. Decroux, J. Muller and R. Flukiger, "The Physical and Structural-Properties of Superconducting A15-Type Nb-Sn Alloys", *J. Mater. Sci.*, Vol. 16, Pages 2145-53, 1981.

[19] X. Xu, M. D. Sumption, S. Bhartiya, X. Peng, and E. W. Collings, "Critical current densities and microstructures in rod-in-tube and tube type Nb_3Sn strands—present status and prospects for improvement," *Supercond. Sci. Technol.*, Vol. 26, Issue 7, 075015, July 2013.

[20] M. T. Naus, "Optimization of internal-tin Nb_3Sn composites", Ph.D. dissertation, University of Wisconsin-Madison, Page 36, 2002.

[21] M. Di. Michiel and C. Scheuerlein, "Phase transformations during the reaction heat treatment of powder-in-tube Nb_3Sn superconductors", *Supercond. Sci. Technol.*, Vol. 20, Issue 7, L55–L58, 2007.

[22] X. Xu, "Prospects for Improving the Critical Current Density of Superconducting Nb_3Sn Strands via Optimization of Nb_3Sn Fraction, Stoichiometry, and Grain Size", Ph.D. dissertation, the Ohio State University, Pages 58-59, 2016.